

Supplementary Information

Label-free Ferrohydrodynamic Cell Separation of Circulating Tumor Cells

Wujun Zhao,^a Rui Cheng,^b Brittany D. Jenkins,^c Taotao Zhu,^a Nneoma E. Okonkwo,^d Courtney E. Jones,^e Melissa B. Davis,^c Sravan K. Kavuri,^f Zhonglin Hao,^g Carsten Schroeder,^h and Leidong Mao^{*b}

^a Department of Chemistry, The University of Georgia, Athens, GA 30602, USA

^b School of Electrical and Computer Engineering, College of Engineering, The University of Georgia, Athens, GA 30602, USA. E-mail: mao@uga.edu

^c Department of Genetics, The University of Georgia, Athens, GA 30602, USA

^d Department of Biological Engineering, Massachusetts Institute of Technology, Cambridge, MA 02139, USA

^e College of Engineering and Computer Science, Syracuse University, Syracuse, NY 13210, USA

^f Department of Pathology, Augusta University, Augusta, GA 30912, USA

^g Department of Medicine, Augusta University, Augusta, GA 30912, USA

^h Department of Surgery, Augusta University, Augusta, GA 30912, USA

Three-dimensional model of ferrohydrodynamic cell separation (FCS)

Cell or bead trajectories are simulated in a three-dimensional (3D) FCS device (relevant dimensions are listed in Fig. S2) by slight modifications of previously developed models with cell properties from cancer cell, white blood cells (WBCs) and relevant beads.^{1, 2} We first calculate the 3D magnetic buoyancy force via an experimentally verified and analytical distribution of magnetic fields as well as their gradients, together with a nonlinear magnetization model of the custom-made ferrofluid. In order to simulate the magnetic field distribution in the channel generated from the permanent magnet, we followed the 3 steps as below:

1. We experimentally measured flux density at the center of magnet's polar surface, and points away from surface to obtain a flux density-distance relationship (see Fig. S1).
2. From measured flux density-distance plot, we determined value of remnant magnetization of the permanent magnet. This value was used in the magnetic field simulation based on a set of governing equations,^{1,3} in order to generate a simulated flux density-distance relationship. We compared the experimental and simulated flux density-distance relationship and they were within 5.81% error range.
3. The simulated magnetic field distribution (flux density, strength, and gradient) was then confirmed to be valid and used in subsequent FCS device optimizations.

The magnetic buoyancy force is expressed as,

$$\vec{F}_m = \mu_0 V_c \left[(\vec{M}_c - \vec{M}_f) \cdot \nabla \right] \vec{H} \quad [S1]$$

where $\mu_0 = 4\pi \times 10^{-7}$ H/m is the permeability of free space, V_c is the volume of a single cell, \vec{M}_c is its magnetization, \vec{M}_f is magnetization of the magnetic fluid surrounding the body, and \vec{H}

is the magnetic field strength at the center of the body.⁴ The magnetization of the ferrofluid \vec{M}_f under an external field \vec{H} is a Langevin function,

$$\vec{M}_f = \left(\coth(\alpha_f) - \frac{1}{\alpha_f} \right) \phi \vec{M}_{f,b} \quad [\text{S2}]$$

where $\alpha_f = \mu_0 \pi M_{f,b} H d_f^3 / 6 k_B T$. $M_{f,b}$ is saturation moments of the bulk magnetic materials, d_f is diameters of magnetic nanoparticles in ferrofluid, k_B is the Boltzmann constant and T is the temperature. ϕ is the concentration (volume fraction) of the magnetic nanoparticles in the ferrofluid.⁴

We also derived the hydrodynamic viscous drag force with velocity difference between the cell and the local flow,

$$\vec{F}_d = -3\pi\eta D_c (\vec{U}_c - \vec{U}_f) f_D \quad [\text{S3}]$$

where η is viscosity of magnetic fluids, D_c is diameter of a spherical cell, \vec{U}_c and \vec{U}_f are velocity vectors of the cell and the fluids respectively, f_D is hydrodynamic drag force coefficient of a moving cell considering the influence with a solid surface in its vicinity, which is referred to as the “wall effect”.⁵⁻⁷ The velocity vectors of the fluids \vec{U}_f were extracted from a 3D velocity profile simulation generated in COMSOL Multiphysics (Version 3.5, COMSOL Inc., Burlington, MA) through an interpolation method. The COMSOL simulation was conducted with exact conditions of experiments.

We finally solved governing equations of motion using analytical expressions of magnetic buoyancy force and hydrodynamic viscous drag force. Because of the low Reynolds number in a microchannel, inertial effects on the particle are negligible. Motion of a non-

magnetic cell in ferrofluids is determined by the balance of hydrodynamic viscous drag force and magnetic buoyancy force.

$$\vec{F}_m + \vec{F}_d = 0. \quad [S4]$$

This equation was solved by using a fourth-order Runge-Kutta time integration scheme in MATLAB (MathWorks Inc., Natick, MA).

We first confirmed the validity of the model by comparing simulated trajectories (Fig. S3) with experimental ones (Fig. S4) that were obtained from imaging 16.9- μm -diameter H1299 cells (emulated with beads of similar size) and 11.1- μm -diameter WBCs in a FCS device. From Fig. S5, the simulated cell trajectories generated by the model matched the experimental one very well. We then started to use the model for FCS optimizations. The dimensions of the channel were listed in Fig. S2. Concentration of ferrofluid was 0.26 % (v/v) and the viscosity was measured to be 2.92 mPa·s. Average diameters of WBC and H1299 cells were 11.1 μm and 16.9 μm . Dimensions of the permanent magnet were 50800 μm (length) \times 12700 μm (width) \times 12700 μm (height) and the B field at the polar surface was measured to be 0.5 T.

Synthesis and characterization of biocompatible ferrofluids. Ammonium hydroxide solution (28%), iron (II) chloride tetrahydrate (99%), iron (III) chloride hexahydrate (97%), nitric acid (70%), iron (III) nitrate nonahydrate (98%), and sodium hydroxide (98%) were purchased from a commercial vendor (Sigma-Aldrich, St. Louis, MO). All reagents were used as received. Maghemite nanoparticles were synthesized by a chemical co-precipitation method.^{8,9} In a typical reaction, 50 mL of ammonium hydroxide solution was quickly added to a mixture of 100 mL of 0.4 M iron (II) chloride tetrahydrate and 0.8 M iron (III) chloride hexahydrate, and was followed by stirring at room temperature for 30 minutes. The suspension was then centrifuged at 2000 \times g for 3 minutes and the precipitate was dispersed in 200 mL of 2 M nitric acid and 0.35 M iron (III)

nitrate nonahydrate. The mixture was maintained at 90 °C for 1 hour. During this time, the color of the mixture changed from black (Fe_3O_4) to reddish brown (Fe_2O_3). The maghemite nanoparticle suspension was centrifuged at 3000×g for 3 minutes and finally dispersed in 120 mL of deionized (DI) water, yielding a stable dispersion with a pH of 1.5-2. The pH of the dispersion was adjusted to 2.9 by 1 M sodium hydroxide solution. 40 mL of Atlox 4913 (Croda, Edison, NJ), a graft copolymer solution, was added to the dispersion and stirred for 5 minutes before raising pH to 7.0. The dispersion was then vigorously stirred at room temperature for 1 hour, and the resulted ferrofluid was dialyzed with a dialysis membrane (Spectrum Labs, Rancho Dominguez, CA) against DI water for one week. DI water was refreshed every 24 hours. After dialysis, excess water was vaporized at 72 °C. Finally, 10% (v/v) 10× Hank's balanced salt solution (HBSS; Life Technologies, Carlsbad, CA) was added into the ferrofluid to render it isotonic for cells followed by adjusting pH to 7.0. Sterile filtration of ferrofluid was performed with a 0.2 μm filter (VWR, Radnor, PA) and ferrofluids were exposed to UV light for 12 hours before experimental use.

Size and morphology of maghemite nanoparticles were characterized via transmission electron microscopy (TEM; FEI, Eindhoven, the Netherlands). Magnetic properties of the ferrofluid were measured at room temperature using a vibrating sample magnetometer (VSM; MicroSense, Lowell, MA) with a 2.15 T electromagnet. The magnetic moment of ferrofluid was measured over a range of applied fields from -21.5 to +21.5 kOe. The measurements were conducted in step field mode at a stepsize of 250 Oe s⁻¹. Zeta potential of the ferrofluid was measured with a Zetasizer Nano ZS (Malvern Instruments, Westborough, MA). The hydrodynamic diameter of nanoparticles was measured by dynamic light scattering (DLS). The

viscosity of ferrofluids was characterized with a compact rheometer (Anton Paar, Ashland, VA) at room temperature.

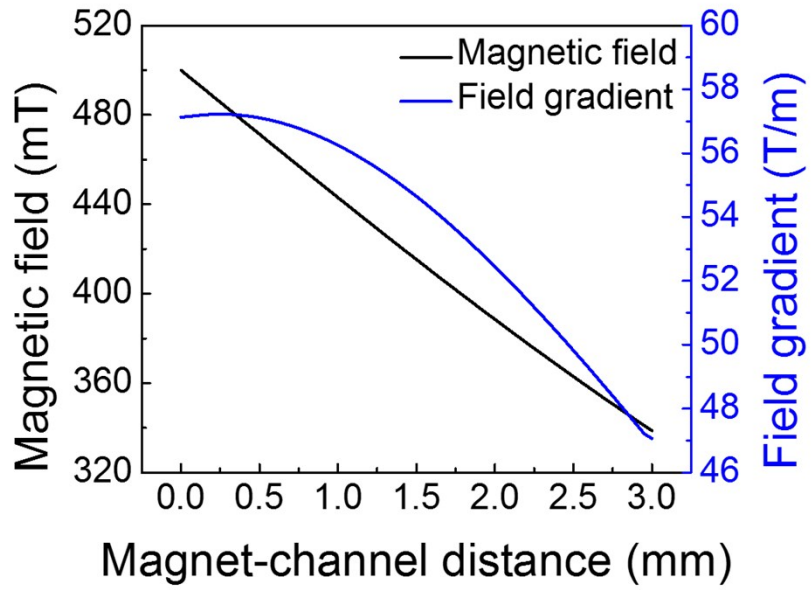


Fig. S1 Measured magnetic field and its gradient of the center of magnet's surface vs. distance between the magnet's surface and the microfluidic channel wall.

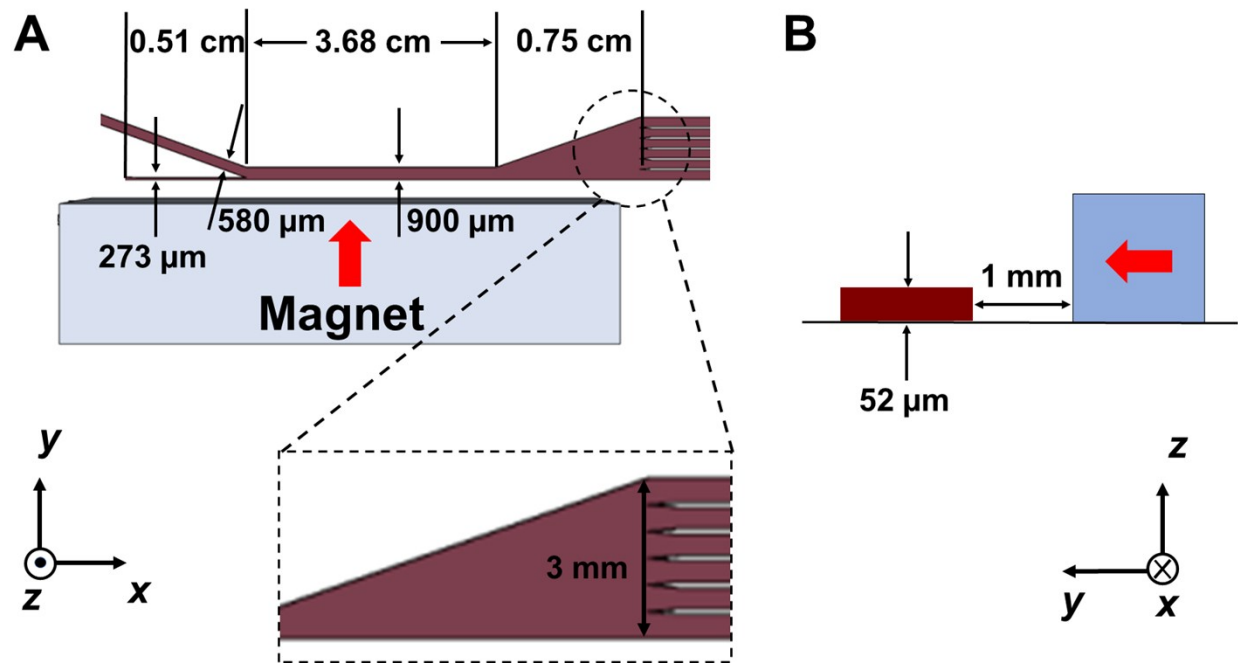


Fig. S2 Schematic and relevant dimensions of a FCS device. (A) Top-view of the FCS device and relevant dimensions. (B) Cross-section view of the FCS device. The red arrow indicates the direction of permanent magnet's magnetization.

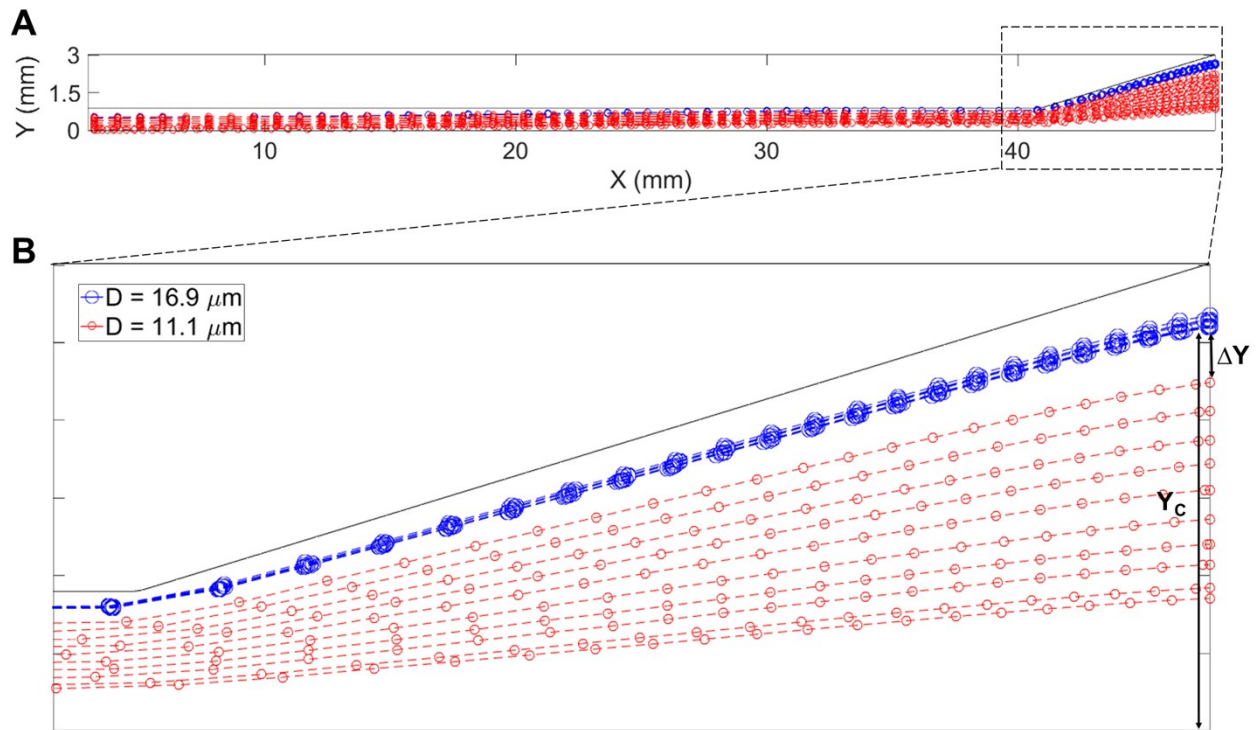


Fig. S3 (A) Cell trajectory simulation of H1299 lung cancer cell (16.9 μm) and WBCs (11.1 μm) in a FCS device. (B) Zoomed-in view of cell trajectories at the end of FCS device. Blue and red trajectories indicate H1299 and WBCs, respectively. Flow rate of cell inlet (Inlet A) was fixed at 6 mL h⁻¹, ferrofluid concentration was fixed at 0.26% (v/v), and magnetic field was fixed at 443 mT and its gradient was fixed at 56.2 T m⁻¹ for this simulation.

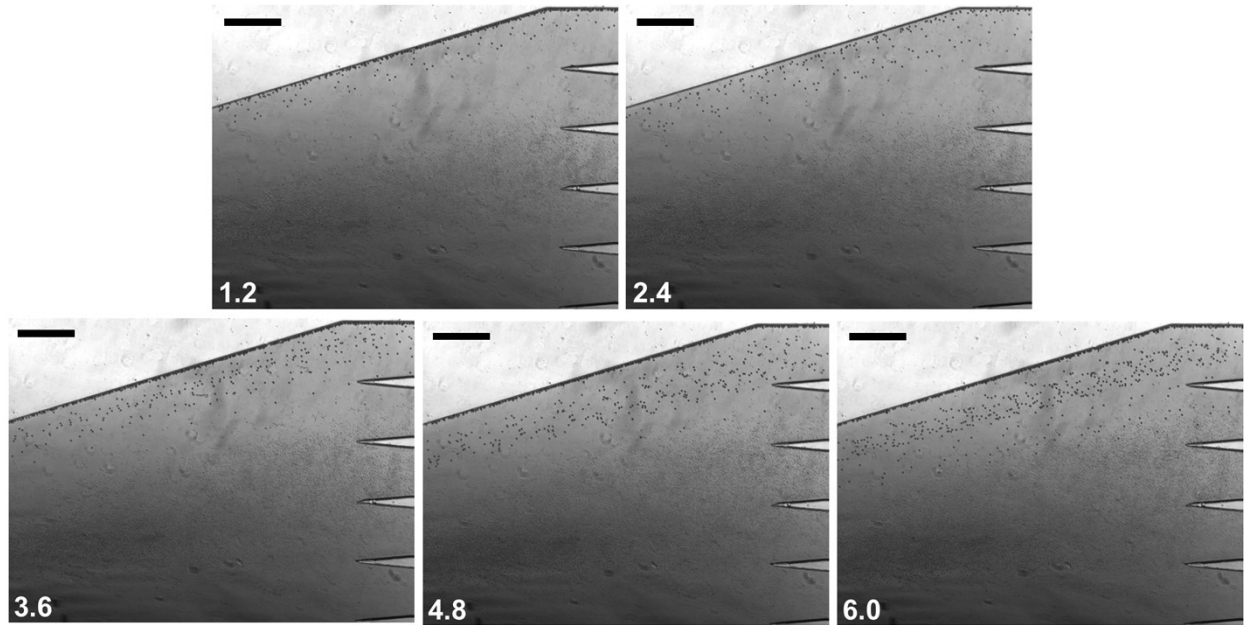


Fig. S4 FCS device calibration with H1299 cells (replaced with beads of similar size, $15.6\ \mu\text{m}$) and WBCs ($11.1\ \mu\text{m}$). The left-bottom number in each figure indicates the associated flow rate of cell inlet A (mL h^{-1}). Flow rate of cell inlet (Inlet A) was fixed at $6\ \text{mL h}^{-1}$, ferrofluid concentration was fixed at 0.26% (v/v), and magnetic field was fixed at $443\ \text{mT}$ and its gradient was fixed at $56.2\ \text{T m}^{-1}$ for this calibration. $\sim 1 \times 10^4$ polystyrene microparticles were mixed with $1\ \text{mL}$ of undiluted WBCs. Scale bars: $500\ \mu\text{m}$.

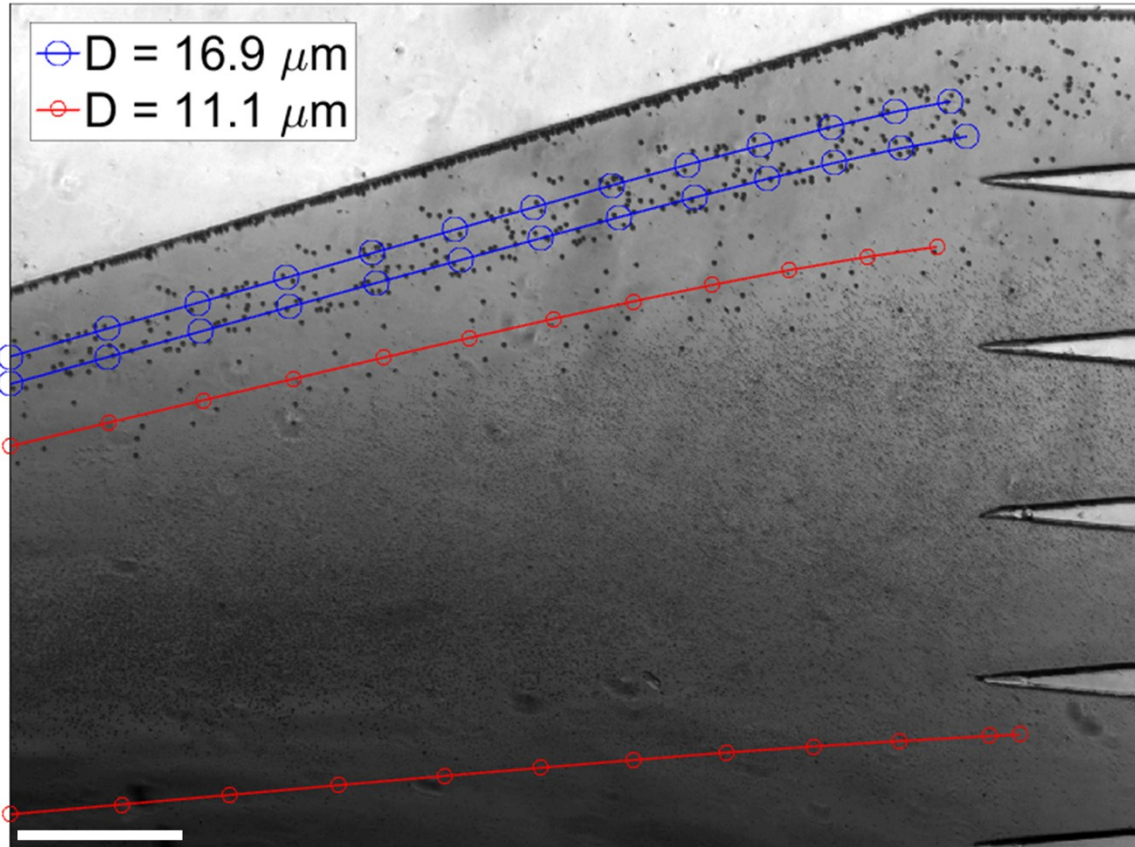


Fig. S5 Comparison of cell trajectories from calibration experiments and simulations of H1299 cells and WBCs at the end of FCS device. Blue lines are the boundary of the simulated H1299 cell trajectory, and red lines are the boundary of the simulated WBC trajectory. The simulated trajectories considered the initial width of microparticle and cell streams at the entry of the channel, therefore had an up and low bound of trajectories. Overall the simulated trajectories matched well with the experimental calibration trajectories, therefore could be used for subsequent FCS device optimization. Flow rate of cell inlet (Inlet A) was fixed at 6 mL h^{-1} , ferrofluid concentration was fixed at $0.26\% \text{ (v/v)}$, and magnetic field was fixed at 443 mT and its gradient was fixed at 56.2 T m^{-1} for simulation and calibration. Scale bar: $500 \text{ }\mu\text{m}$.

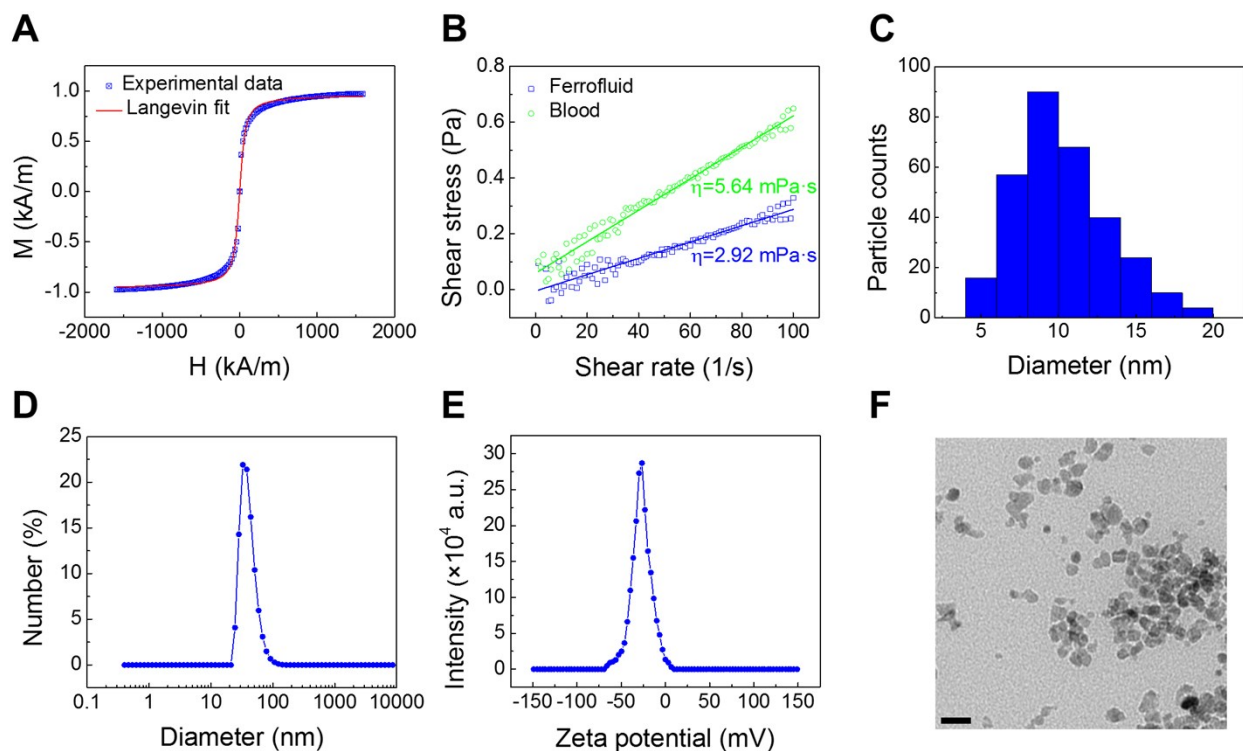


Fig. S6 Characterization of custom-made ferrofluids. (A) Magnetization of the as-synthesized ferrofluid. Solid red lines are the fitting of the experimental data to the Langevin function. Saturation magnetization of this ferrofluid was 0.96 kA m^{-1} , corresponding to a 0.26 volume fraction or concentration. (B) Rheological plots of the ferrofluid and blood. The viscosity of ferrofluid was measured to be $2.92 \text{ mPa}\cdot\text{s}$. (C) Size distribution of maghemite nanoparticles within the ferrofluid ($d=11.24 \pm 2.52 \text{ nm}$). (D) Size distribution of maghemite nanoparticles was measured by dynamic light scattering (DLS). Hydrodynamic diameter was $40.77 \pm 12.71 \text{ nm}$. (E) Zeta potential of ferrofluid was measured to be $-27.2 \pm 11.4 \text{ mV}$, indicating a negative surface charge on the particles. (F) A transmission electron microscopy (TEM) image of the maghemite nanoparticles. Scale bar: 20 nm .

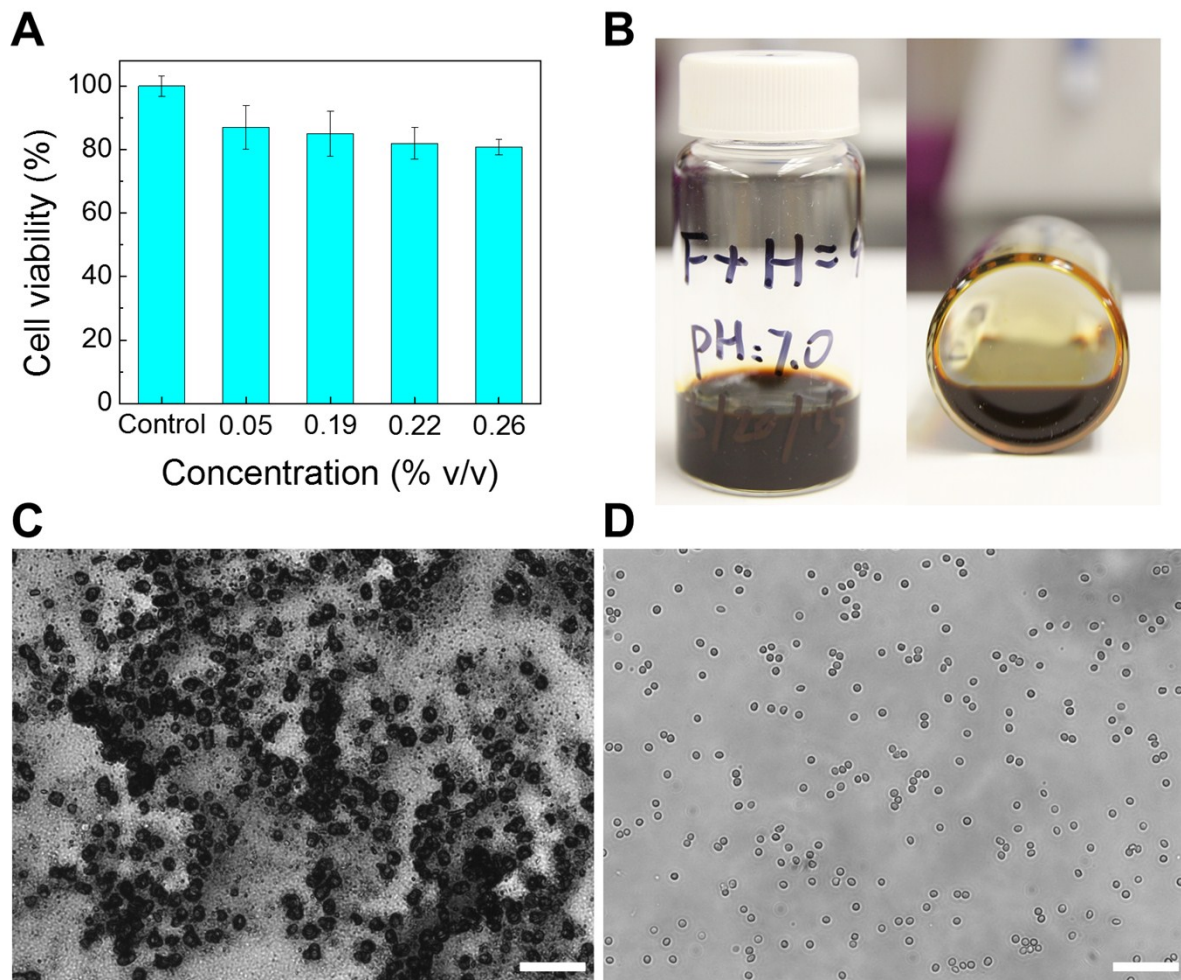


Fig. S7 (A) Cell viability of H1299 lung cancer cells in different concentrations of ferrofluids was evaluated by a MTT assay. Cell viability was $80.8 \pm 2.4\%$ after 12-h incubation with a 0.26% (v/v) concentration ferrofluid. (B) Colloidal stability of biocompatible ferrofluids. The maghemite nanoparticles remained colloidal stable for at least 10 months in solution and there was no visible precipitation over time. (C) Blood cells, mixed with a commercial water-based ferrofluid, showed an irreversible flocculation. (D) No flocculation or aggregation of blood cells was found within the biocompatible ferrofluid. Scale bars: 50 μm .

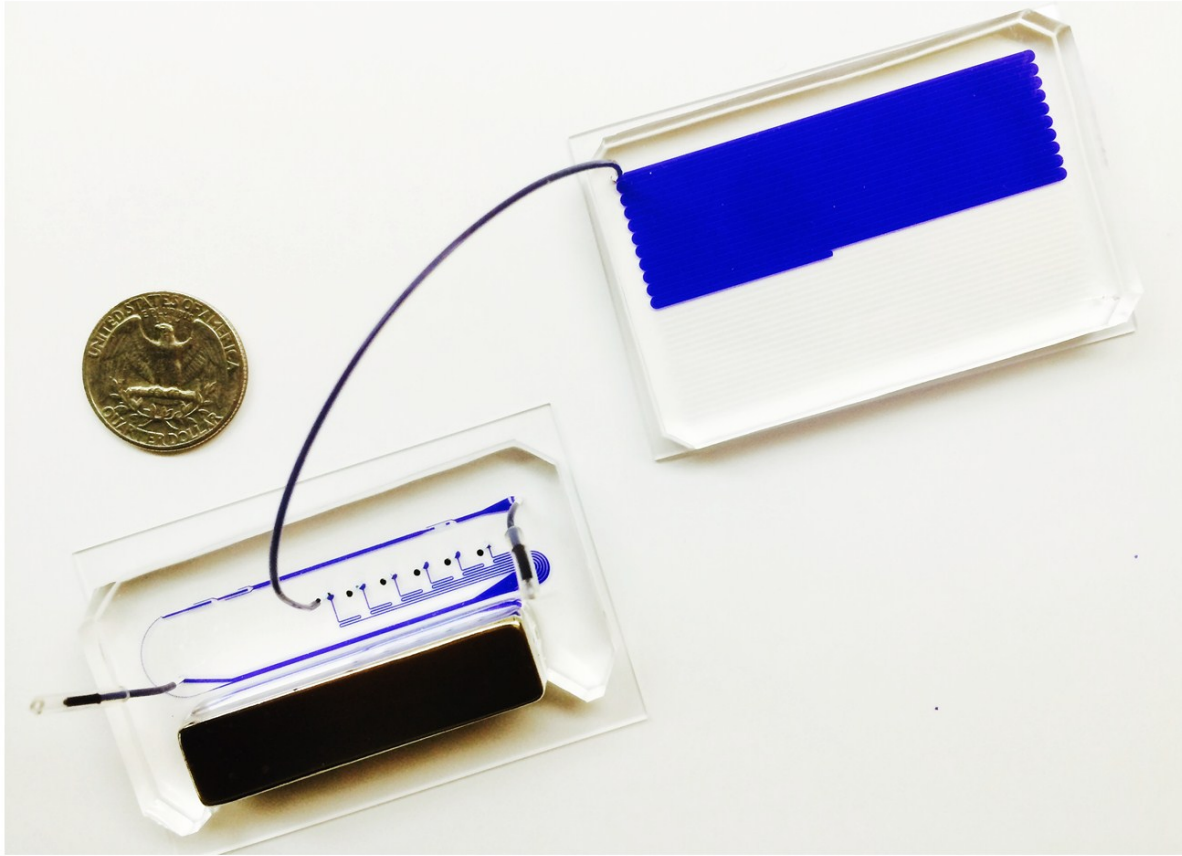


Fig. S8 An image of a FCS device and an attached collection chamber. The FCS device was connected to a serpentine collection chamber that was used to accurately enumerate cancer cells for the FCS calibration using cultured cancer cell lines. The depth of collection chamber is 50 μm . The size of the glass slide is 75 \times 50 mm. Blue dye was used to visualize the microchannel.

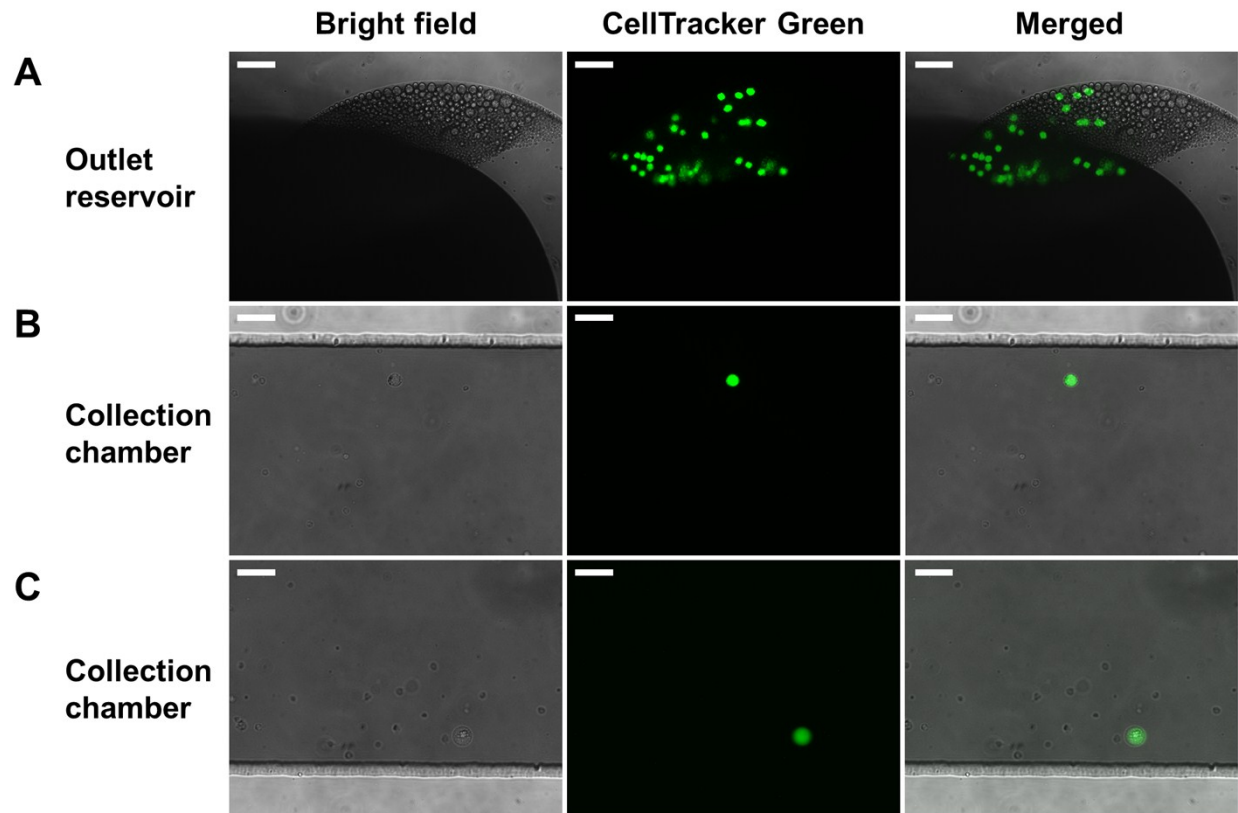


Fig. S9 Representative micrographs of lung cancer H1299 cells and WBCs after a separation of spiked cancer cells in a FCS device at a throughput of 6 mL h^{-1} . ~ 100 CellTracker Green stained H1299 cells were spiked into 1 mL of undiluted WBCs. (A) H1299 lung cancer cells and WBCs were identified in the outlet (outlet 6) reservoir. Scale bars: $100 \mu\text{m}$. (B) and (C) H1299 lung cancer cells and WBCs were identified in the serpentine collection chamber. Scale bars: $50 \mu\text{m}$.

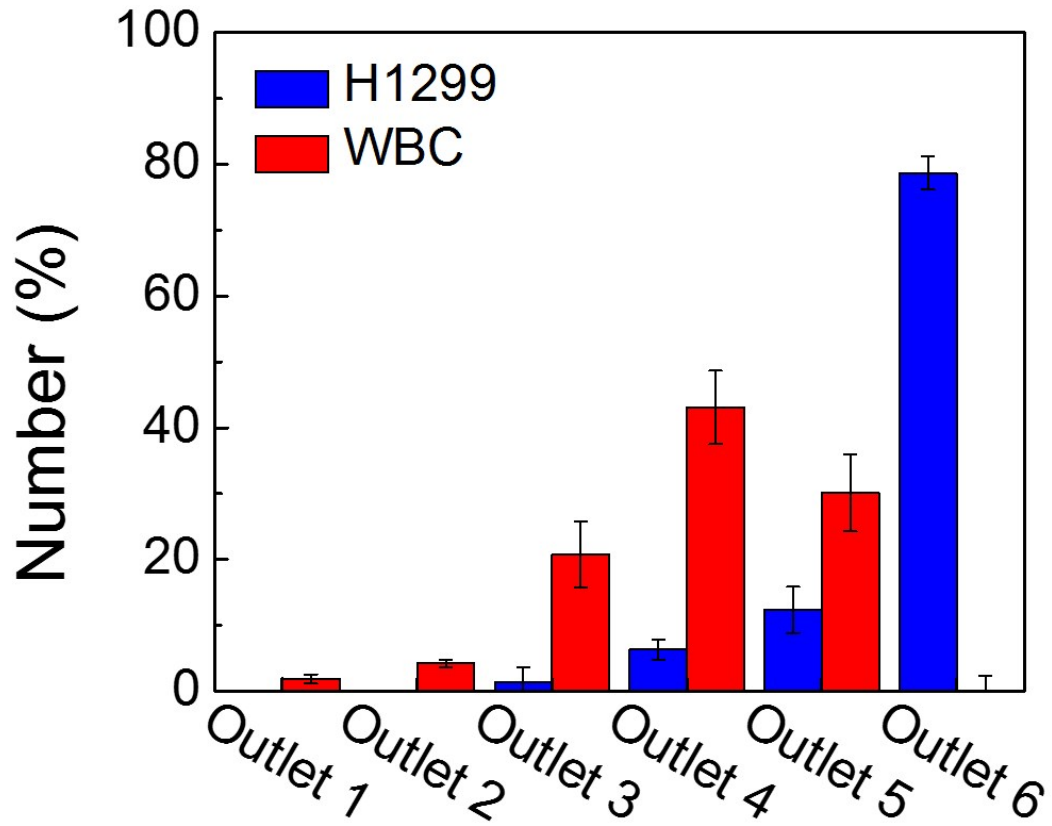


Fig. S10 Cell type distribution of cells collected from outlets 1-6 after a separation of ~100 H1299 cells spiked into 1 mL of undiluted WBCs using a FCS device at a throughput of 6 mL h⁻¹.

A

Cell type	Average cell size (μm)
H1299	16.9
A549	15.5
H3122	17.8
PC-3	18.9
MCF-7	18.7
HCC1806	17.6
WBC	11.1

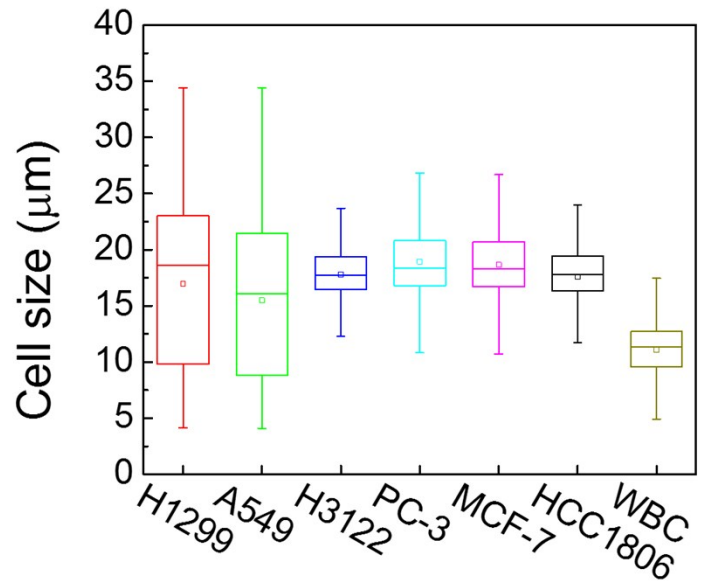
B

Fig. S11 (A) The average cell size of six cancer cell lines and WBCs measured by a cell counter. (B) Size distribution of cancer cells and WBCs.

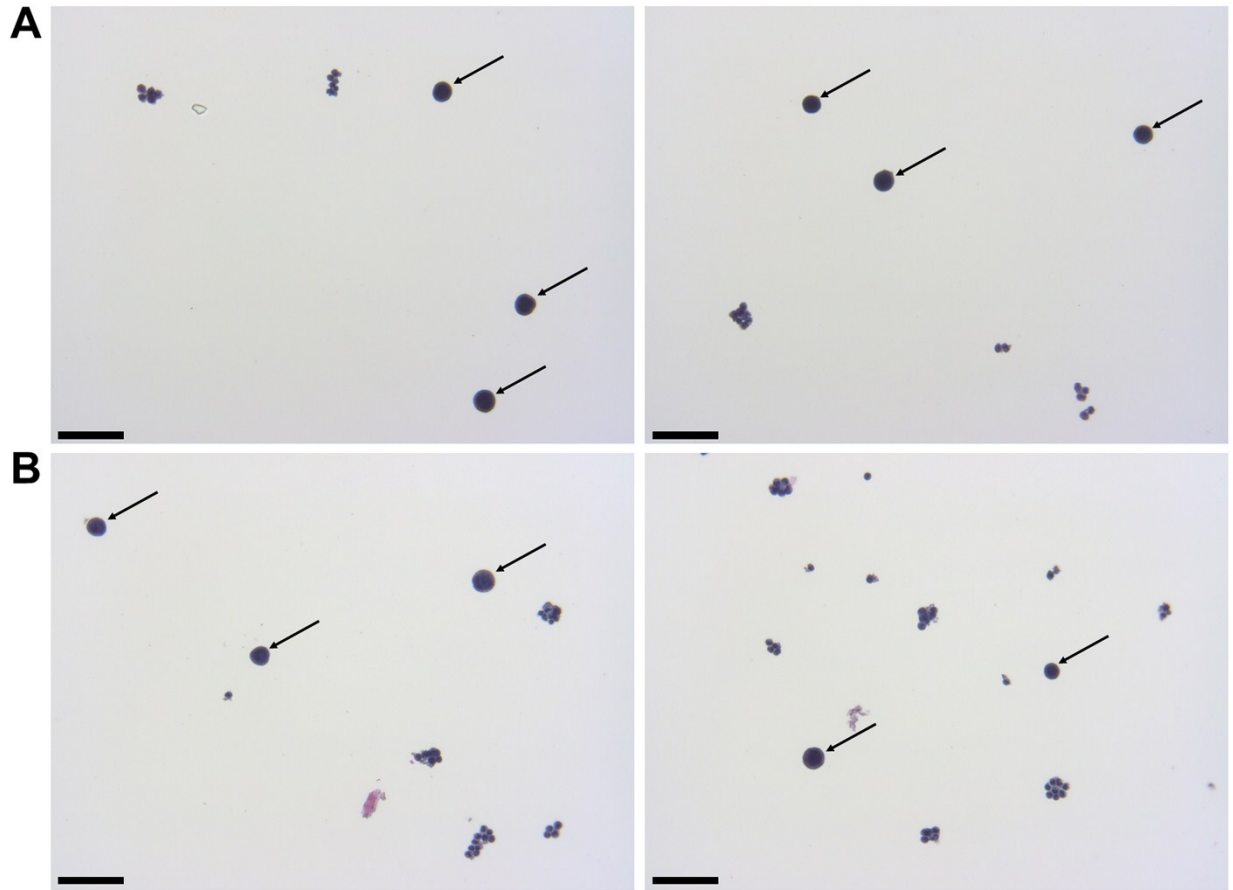


Fig. S12 Representative images of CTC identification from patient A and B, with their blood processed by FCS devices. Black arrows indicate the identified CTCs. Scale bars: 50 μ m.

References:

1. R. Cheng, T. T. Zhu and L. D. Mao, *Microfluid Nanofluid*, 2014, **16**, 1143-1154.
2. T. T. Zhu, D. J. Lichlyter, M. A. Haidekker and L. D. Mao, *Microfluid Nanofluid*, 2011, **10**, 1233-1245.
3. E. P. Furlani, *Permanent magnet and electromechanical devices : materials, analysis, and applications*, Academic, San Diego, Calif. ; London, 2001.
4. R. E. Rosensweig, *Ferrohydrodynamics*, Cambridge University Press, Cambridge, 1985.
5. P. Ganatos, S. Weinbaum and R. Pfeffer, *J Fluid Mech*, 1980, **99**, 739-753.
6. G. P. Krishnan and D. T. Leighton, *Phys Fluids*, 1995, **7**, 2538-2545.
7. M. E. Staben, A. Z. Zinchenko and R. H. Davis, *Phys Fluids*, 2003, **15**, 1711-1733.
8. W. J. Zhao, T. T. Zhu, R. Cheng, Y. F. Liu, J. He, H. Qiu, L. C. Wang, T. Nagy, T. D. Querec, E. R. Unger and L. D. Mao, *Advanced Functional Materials*, 2016, **26**, 3990-3998.
9. R. Massart, *Ieee T Magn*, 1981, **17**, 1247-1248.